Applied Physics B: Lasers and Optics manuscript No.
(will be inserted by the editor)

Generation of THz radiation using bulk, periodically and aperiodically poled lithium niobate.

Part 2: Experiments

J. A. L'huillier[1]⋆, G. Torosyan[2], M. Theuer[2], C. Rau[1], Yu. Avetisyan[3], R. Beigang[1,2]

[1] Technical University of Kaiserslautern, Dept. of Physics, Erwin-Schroedinger-Strasse 46, 67663 Kaiserslautern, Germany
[2] Fraunhofer IPM, Terahertz Measurement and Systems, Erwin-Schroedinger-Strasse 46, 67663 Kaiserslautern, Germany
[3] Microwave Eng. Dept. Yerevan State University, 1 Alek Manoogian Str., Yerevan, 375049, Armenia

Received: date / Revised version: date

Abstract Optical rectification of femtosecond pulses in nonlinear materials is an efficient method to generate ultra short terahertz (THz) pulses in a wide frequency range extending from 100 GHz to well above 10 THz. Lithium niobate (LN) is well suited for such purpose despite the high absorption in the THz range. In this part we will focus on the various experimental realizations to produce THz radiation in bulk, (a)periodically and two dimensionally poled LN. The possible bandwidth, tunability and the techniques to overcome the high absorption will be discussed as well.
PACS: 42.65.Ky, 42.70.Mp, 42.72.Ai

1 Introduction

The generation and application of THz radiation using photonic techniques has attracted considerable interest over the past years. Among the different optical techniques of THz generation the optical rectification (OR) of fs-laser pulse in a nonlinear crystal, i.e. difference frequency generation (DFG) between frequencies within the broad spectrum of the same pulse has turned out to be extraordinary well suited.
In part one[1] of this review the possibility of THz emission was theoretically considered taking into account a direction different from the fs-pulse propagation. From this discussion it is clear that the main difference in the various schemes of OR to generate THz radiation is the way to achieve phase-matched THz generation and to reduce the THz wave decay in the nonlinear crystal. While the first part focussed on the theoretical description, the following discussion will focus on the experimental realizations of the theoretical concepts discussed in part one.
Similar to the outline of part one we will discuss the various methods in bulk materials and proceed afterwards with one dimensional QPM structures (ppLN, AppLN) and two dimensional QPM structures (TppLN).
Beginning with ferroelectric materials like lithium niobate (LN) [2–8] or lithium tantalate[9] over semiconductor materials like GaAs [10,11], GaSe [12,13] or $ZnGeP_2$[14] to organic materials like the organic salt DAST (4-dimethylamino-N-methyl-4-stilbazolium-tosylate) [15,16] or polymeres [17,18], a wide range of different materials have been used for THz generation by OR of fs-laser pulses. All of these materials have particular advantages and inherent difficulties.
As a nonlinear material LN has turned out to be extraordinarily well suited for this purpose. This is because of its high nonlinearity [19,20], high transparency in the visible and near infrared spectral region [21] and the well developed poling technique [20,22,23] for this material. The major drawback of this material is the high absorption at THz frequencies [24,25]. The intensity absorption coefficient α increases from around 12 cm^{-1} at 1 THz to more than 170 cm^{-1} at 2.5 THz [25,26]. The main origin of this strong absorption is the low frequency tail of the transverse optical phonon mode at 7.6 THz[25,27]. Recently published detailed measurements performed by L. Plfalvi et al.[24] show that the absorption depends on the stoichiometry and on the MgO doping concentration, which is often used to reduce the photorefractivity of LN. The absorption decreases in 0.7 %Mg doped stoichiometric LN (sLN) to 82.6cm^{-1} at 2.4 THz, which is still considerable higher than the absorption in the visible (VIS) or near-infrared (NIR). An significant reduction of the absorption can be achieved by cooling to cryogenic temperatures[24]. This method was utilized to enhance the THz wave output[28], but is hardly practicable for many applications. Therefore concepts to minimize the path length inside the crystal, are still of high interest.

⋆ *Fax: +49-631-205-3906, E-mail: huillier@physik.uni-kl.de*

Due to the high dielectric contribution of the transverse optical phonon mode to the refractive index, the value of the refractive index in the THz range is more than twice as high as the refractive index in the NIR or VIS. Therefore it is difficult to use the natural birefringence to obtain phase matching in LN for efficient THz generation.
Despite these problems the material properties of LN are still a reasonable compromise for the requirements for a THz source based on frequency conversion of NIR radiation. The remaining constrains have been partly overcome by various concepts to reduce in particular the high absorption of LN. This is one reason why this material is still widely used for THz generation. Therefore we focus the discussion exemplary to LN.

2 Experimental setup

The typical experimental setup used in the experiments is shown in Fig. 1. The setup consists of a Ti:Sapphire laser (Spectra Physics, Tsunami), which provides sub $100fs$ pulses with a repetition rate of 80 MHz and an average power of $\sim$ 1.5 W. The collimated laser beam is splitted into two beams. One is used to trigger the detector behind a delay line and the other beam is focused into the sample. The crystal is positioned within the Rayleigh length of the focus of the NIR radiation. The emitted THz radiation is collected and focused by two spherical silver mirrors onto the detector. The detector was a standard SOS or LT-GaAs photoconductive antenna with a typical dipole length of 50 μm. Using two sets of mirrors, Mf and Ms, the THz radiation in forward direction and a direction perpendicular to the surface can be observed respectively.
Beside the observation direction the various realizations differ in the type or structure of the nonlinear medium LN. A detailed discussion of the particular structures will be given in the corresponding section.

3 Bulk lithium niobate (LN)

3.1 Optical rectification

As early as 1962 optical rectification in electro-optic media was reported[29]. Optical rectification of fs-pulses is in fact collinear difference frequency generation between particular spectral components within the ultra-short laser pulse[30]. In 1992 Xu et al. [31] investigated the generation of THz radiation in electro-optic materials (here LN and $LiTaO_3$) due to the interaction with fs optical pulses. Two years later Carrig et al. compared the efficiency of LN, $LiTaO_3$ and DAST[32] and reported on the powerscaling of THz radiation. These results showed despite the low damage threshold of DAST that the performance is superior to LN and $LiTaO_3$. Further experimental realizations of this scheme have been demonstrated in many experiments. But in this case of non phasematched DFG the THz radiation is emitted only from entrance and exit surfaces of the crystal within the coherence length defined by

$$l_c = \frac{\pi}{\omega_{THz}} \cdot \frac{c}{|n_g - n_{THz}|}. \tag{1}$$

With typical values for both refractive indices in LN ($n_g = 2.3$ and $n_{THz} = 5.17$[25]) the coherence length is $\sim 50\mu m$ and therefore only a small part near both surfaces of the crystal is used. A sketch of a typical crystal and the coordinate system is shown in Fig. 2.
For the comparison with the other methods discussed in this publication we used a 1 mm thick x-cut LN crystal to produce THz radiation. Fig. 3(a) shows the electric field of the generated pulses. As expected the electrical field in the time domain consist of two cycles. The delay between the two peaks is $\Delta t = 9.5ps$. Due to the simple relationship between the length of the crystal and the delay time[1,31]

$$\Delta L = \frac{c}{\Delta n} \cdot \Delta t \tag{2}$$

this results in $\Delta L = 1mm$ which is in good agreement with the sample length L. The amplitude of the second peak (larger delay) is smaller than the amplitude of the first peak (shorter delay). This behavior can easily be understood if we take the absorption and the refractive index of LN in the THz range into account. Since the refractive index of LN is around 5.1 in the THz range the second cycle corresponds to the radiation generated at the entrance facet of the sample (See also the theoretical discussion in part one[1]). The radiation forming the second peak took a path length of $\approx 1mm$ in LN while the first peak is generated very close to the exit surface. Therefore higher absorption losses occur for the second peak resulting in a lower amplitude.
The Fourier transform gives the spectrum shown in Fig. 3(b). The obtained spectrum covers a frequency range of $\approx$ 1.6 THz. The envelope is related to the pulse duration of the Fourier limited fs-pulse (see part one[1]). The measured bandwidth is limited mainly by the bandwidth of the fs-pulses and the bandwidth of the detector. In addition the absorption strongly increases for higher frequencies, resulting in a further limitation of the bandwidth. This behavior will be discussed in detail in section 3.2.
In opposite to the envelope the oscillations result form destructive interference of particular frequency components. The destructive interference occur for components whose coherence length fit $2 \cdot n$ times into the crystal length (with an integer n).
Despite the high absorption of LN for THz frequencies[24,25] in this scheme only small absorption losses for first THz-pulse (first peak in Fig. 3 a) occur, due to the generation very close to the exit surface. But the generated power for DFG scale with the square of the interaction length up to the coherence length. Due to

the short coherence length the generated power for non phasematched DFG is strongly limited.

3.2 Cherenkov radiation

To improve the THz generation output it is necessary to obtain phase matching between the participating waves. One way is to use Cherenkov radiation. The analogue of the Cherenkov radiation from superluminal charged particles for intense light pulses has been predicted by Askaryan already in 1962 [33]. More than 20 years later the effect was demonstrated experimentally [34,35] for microwave and THz wave generation by pumping with ultra short optical pulses.
When the wave packet of an ultrashort optical pulse propagates through a bulk of electro optical material, the generated Cherenkov radiation composes a cone around the direction of propagation. In this case under a single defined angle to the direction of the NIR beam the particular THz waves generated at different points in the crystal are in phase. This angle is called the Cherenkov angle Θ_C and it is given by (see also part one[1]):

$$\Theta_C = \arccos\left(\frac{n_g}{n_{THz}}\right). \tag{3}$$

For typical values of the group index of LN in the NIR $n_g = 2.3$ and the refractive index at a frequency of $1\ THz$ of $n_{THz} = 5.17$ the angle is $\Theta_C = 63.6°$.
As a consequence the THz radiation hits the surface of a conventional rectangular shaped LN crystal under an angle of $\approx 26°$ to the normal. Due to the very high refractive index of LN in the THz range the angle of total reflection is only around 11°. The THz radiation is therefore totally reflected and absorbed inside the LN crystal. To allow the THz radiation to exit the crystal-air interface in normal direction without refraction, one has to take special care. Hu et al.[36] used a setup where the exciting laser beam has an incident angle of $< 27.4°$. The refraction of the beam at the crystal-air boundary results in a propagation direction not parallel to the crystals boundary. By changing the incident angle the angle between the emitted Cherenkov radiation and the exit surfaces can be adjusted suitably. But in this setup only a limited length can be used.
To avoid this problem typically a plate with wedged exit surfaces is used. In the case of LN the wedge angle is about 26°. So the THz radiation can pass the surface. This is schematically shown in Fig 4 (a). However, the path length of the generated radiation inside the crystal and therewith the absorption losses increases, since the radiation is not produced close to the surface.
For a further improvement of the output coupling efficiency and spectral bandwidth the wedged part of the crystal can be replaced by a silicon prism[6]. A schematic of this geometry is show in Fig. 4 (b). This setup was originally developed by K. Kawase et al.[37] for the extraction of THz radiation out of a ns pumped THz-OPO in a non collinear setup. The absorption for the THz radiation in silicon is much lower and the refractive index ($n \sim 3.4$ [38]) is in between the refractive index of air and LN. So the THz radiation can pass the surfaces without total internal reflection and less fresnel losses. If the NIR beam is placed near the interface between the LN crystal and the silicon prism, the absorption in LN is minimized.
For the experimental comparison of both schemes again the setup shown in Fig.1 is used. The sample was replaced by a wedged crystal, the sideways detection was used and the detection geometry was adjusted accordingly.
The experimentally obtained electrical field amplitude and spectrum for the first scheme, shown in Fig 4 (a), are plotted in Fig 5 (a) and 5 (b) respectively.
The electrical field amplitude consists as expected of one single cycle and the spectrum covers more than 4 THz limited by the spectral bandwidth of both the pump pulse and the detector. The spectrum shows various absorption lines of water. During the experiments no special care was taken to remove the water vapor out of the air, because these absorption lines do not disturb the aimed comparison of the different generation schemes.
In Fig. 6 (a) and (b) the experimentally obtained spectra for a wedged MgO:LN crystal (solid line) and MgO:LN sample with a silicon prism as an output coupler (dotted line) are shown for two different focal lengths[6].
From a comparison of the different focal lengths it is obvious that a shorter focal length result in a broader spectrum. This is the expected result from the theoretical discussion[1]. In addition it is seen that the obtained bandwidth of the THz radiation with the wedged sample is smaller compared to the setup with the Si-prism. This behavior can be easily understood, if we take into account the strong and frequency dependent absorption. The absorption strongly increases for higher THz frequencies[25]. This results in a smaller amplitude for higher THz frequencies compared to the obtained amplitude for lower THz frequencies.
The frequency depended absorption can be included in the theoretical description (see Eqn. (21) in part one[1])by adding an exponential factor (Beer's absorption law). For simplicity we assume a constant path length s inside LN for the THz radiation generated at different points of the crystal. This is at least valid for the setup with the silicon prism. With this assumption, we obtain:

$$E_\Theta(\omega, R, \Theta_x) \sim G'(\omega, \Theta_x) \cdot F(\omega, \Theta_x) \cdot e^{-\frac{\alpha(\omega)}{2} \cdot s} \tag{4}$$

with the releations $G'(\omega, \Theta_x) = G(\omega, \Theta_x) H(\omega, r_0)$ and $F(\omega, \Theta_x) = sinc\left(\frac{\omega L \Delta n}{2c}\right)$ given in part one [1]. $\alpha(\omega)$ denotes the intensity absorption coefficient.
With the empirical relation and experimental data for the frequency depended absorption $\alpha(\omega)$ obtained by

M. Schall et al.[25] an analytical calculation is possible. Fig. 7 shows the calculated spectra for different path lengths inside LN. The calculation was performed with Eqn. (4) and the pulse duration ($\tau = 100$ fs) and the beam waist ($\omega_0 = 30$ μm) used in the experiments.
From Fig. 7 it is clear that with an increasing path length inside LN the amplitude and the bandwidth decreases and the maximum of the electrical field moves towards lower frequencies. This is the expected behavior caused by the increasing absorption at higher THz frequencies. A further problem arises from the fact that the beam width of the NIR beam should be in the order of the THz wavelength to obtain constructive interference between the partial waves generated at different points. To obtain a reasonable bandwidth and power it is necessary to obtain a small focus in the medium. Therefore the power scaling in this scheme is limited due to radiation damage.

4 Periodically poled lithium niobate (ppLN)

Phase matching for optical nonlinear processes in the visible and NIR spectral range is normally obtained by birefringence phasematching[39], by quasi phase matching in periodically poled ferroelectrics[40] or a combination of both[41].
In fact the natural birefringence of GaSe has been used to obtain phase matching for the generation of FIR radiation[42]. But phase matching using the natural birefringence is difficult or even impossible below but close to the phonon frequency[43].
While birefringence phase matching is not preferable, quasi phase matching is still a versatile possibility[4,7, 44–48]. In contrast to optical rectification and Cherenkov radiation obtained from bulk LN, THz generation in ppLN leads to tunable narrow band THz radiation.
A sketch of a periodically poled crystal is shown in Fig. 8. The necessary poling periods vary between 10 microns (10 THz) and 400 microns (300 GHz). In the theoretical discussion[1] an analytical relation between the poling period Λ and the center frequency $\nu = \frac{\omega}{2\pi}$ of the THz radiation was obtained (see Eqn. (28) in part one), which can be written in the form:

$$\Lambda = \frac{1}{\nu} \cdot \frac{c}{|n_g - n_{THz}(\nu)\cos\Theta|} \tag{5}$$

The angle Θ describes the direction of observation. An angle of $\Theta = 0$ and $\Theta = \pi$ corresponds to emission in forward and backward direction, respectively.
Please note that the refractive index in the THz range varies between 5.17 at 1 THz and 5.8 at 3 THz[25] while the variation of the refractive index between the particular components of the NIR fs-pulse is very small.

4.1 forward and backward emission

The generation of narrowband THz radiation by quasi phasematched OR in ppLN was first reported by Y. S. Lee and coworkers[44,45].
They found in addition to the THz emission in forward direction ($\Theta = 0$) an additional emission in backward direction ($\Theta = \pi$). For a typical poling period of $\Lambda = 120\mu$m the calculation results in a THz frequency of 0.87 THz and 0.34 THz for forward and backward direction, respectively.
QPM structures allows a definition of both the center frequency (see Eqn. (5)) and the bandwidth. For the experimental realization the setup for the forward direction is used (mirrors Mf, see Fig. 1). The setup is very similar to the setup for optical rectification in bulk LN (see section 3.1). Only the bulk LN crystal has been replaced by a ppLN sample. The typical crystals used for our investigations had a poling period of $\Lambda = 120\mu m$. The samples were 0.5 mm thick and had a length of 10 mm. Fig. 9 (a) and (b) shows the experimentally and numerically obtained electrical field in the time domain observed in forward direction.
From Fig. 9 it is clear that the amplitude of the electrical field decreases exponentially with an increasing delay. This behavior can easily be understood if again the different velocities and absorption for the NIR and the THz radiation is considered. The NIR radiation is much faster than the THz radiation. Therefore the radiation generated in the poling period at the exit surface of the ppLN crystal arrives at first at the detector. In addition due to the shortest path length inside the crystal the lowest absorption occurs and therefore the largest electrical field amplitude is obtained. With an increasing path length inside the ppLN crystal the delay and the absorption increases. Similar to the discussion in section 3.2 the high absorption can be included into a quantitative approach by considering an exponential factor (Beer's absorption law) to the theoretical description. This additional factor results in the observed decay of the field amplitude for longer path length inside the crystal.
The number of cycles of the electrical field corresponds to the number of periods which contribute to the electrical field[1]. Therefore from the 40 visible cycles in Fig. 9(a) a usable crystal length of 4.8 mm can be calculated. This means that the usable length for the THz generation is strongly limited by the high absorption of LN, while the usable length for applications of ppLN in the VIS or NIR spectral range is limited mainly by the poled crystal length.
For a comparison of the experimentally obtained electrical field and the theoretical prediction the numerically calculated electrical field is shown in Fig. 10 (b). To compare the numerical and experimental results the graph from Fig. 9 (a) is filtered to suppress the oscillations caused by the emission in backward direction and is also plotted in Fig. 9 (b). To obtain a reasonable agree-

ment between theory and experiment a poling period of $\lambda = 120.7\mu m$ and an absorption which is a factor of 1.4 higher than in the measurements of M. Schall et al.[25] was used for the calculation. The first correction can be explained by a slightly rotated crystal and the second correction may attributed to the crystal and its composition in this particular case.
Fig. 10(a) and (b) show the spectrum calculated by a Fourier transformation of the electrical field. From Fig. 10(b) it is obvious that the theoretical and experimental results fit very well. The theoretical center frequency ν calculated by Eqn. (5) using the parameters $\Lambda = 120.7\mu m$, $\Theta = 0$, $n_g = 2.3$ and $n_{THz} = 5.17$ is $\nu = 0.866THz$. This is in good agreement with the experimental result. Beside the main peak in Fig. 10(a) a second peak at 0.32 THz is observed. This frequency is close to the expected frequency of THz radiation generated in backward emission. Therefore this radiation can be attributed to THz radiation generated in backward direction. But please note that the radiation emitted in backward direction is detected in forward direction. This can be explained by two possible schemes. In the first scheme (A) the THz radiation generated in backward direction is partially reflected at the entrance surface of the LN crystal. In opposite to scheme (A) in scheme (B) the NIR radiation is partially reflected at exit surface of the crystal. The NIR radiation propagating from the exit surface backward to the entrance surface generates THz radiation similar to the THz radiation in backward direction in scheme (A). This radiation is the observed radiation in forward direction.

4.1.1 Frequency tuning Frequency tuning of the radiation generated by quasiphasematched nonlinear optical processes can be obtained by changing the poling period or the temperature [46]. Different ppLN crystals of various poling periods for the generation of THz radiation in a wide range of wavelengths have been used. It is known that various discrete poling periods on a single crystal can be fabricated [49]. The selection of the THz frequency in such a multigrating ppLN crystal can be done by moving the crystal perpendicular to the NIR beam. But this scheme allows only the selection of a few discrete frequencies. Further fine tuning can be done by changing the temperature of the sample [46].
Experimentally obtained and theoretically calculated frequencies for various poling periods for the THz generation in forward as well in backward direction are plotted in Fig. 11. Besides the results for first order QPM also the results for third order QPM in forward direction are shown. With poling periods between $10\mu m$ and $400\mu m$ the complete THz range between 0.24 THz and 10 THz can be generated.
Besides using different discrete poling periods a further possibility to continuously tune the poling period is to rotate the crystal [7]. In Fig. 12 a schematic diagram of the used setup is shown. The pump beam passes through the center of the round crystal (which is also the axis of rotation) so that the beam direction stays constant during the rotation of the crystal. In this way any beam deviation during rotation can be avoided. The effective poling period changes with $1/cos(\alpha)$ where α is the angle between the direction of beam propagation and the normal to the poling direction and therefore the center frequency of the THz radiation generated in forward direction is given by a modified Eqn. (5):

$$\nu(\alpha) = \nu(0)\cos\alpha = \frac{\cos\alpha}{\Lambda} \cdot \frac{c}{|n_g - n_{THz}(\nu)|} \qquad (6)$$

With an increasing rotation angle the effective length of the poling period increases, but the number of contributing domains decreases. Eqn. (6) is valid for small rotation angles as long as a reasonable number of periods contribute to the THz generation.
Due to the decreasing number of contributing domains, the relative bandwidth increases accordingly. The bandwidth can be calculated form the equation obtained for ppLN crystals by considering the rotation angle α:

$$\frac{\Delta\nu}{\nu} = \frac{1.768}{N} \cdot \cos\alpha. \qquad (7)$$

For the experimental demonstration a round ppLN crystal with a diameter of 7.5 mm and a poling period of 127 μm was used [7]. Fig. 13 shows the experimentally obtained tuning curves for the THz frequency (upper graph) and the relative bandwidth (lower graph). The solid line represents the theoretically calculated tuning characteristics and the bandwidth in the upper and lower graph, respectively. In this experiment a continuous tuning range between 0.18 THz and 0.82 THz with a minimum relative bandwidth of 2.5 % has been demonstrated.

4.2 surface emission

One major drawback of the quasi phase matched collinear optical rectification discussed above is the inherent long path length inside the crystal. The strong absorption of LN reduces the available output power and limits the number of domains that effectively participate in the THz generation. Last, according to Eqn. (7), results in a worsening of the monochromaticity of the generated THz wave. A possible solution of this problem is the emission of the generated THz radiation perpendicular to the surface of the ppLN crystal. In this way the path length within the ppLN crystal can be reduced considerably and the area of THz emission can be enlarged, resulting in a smaller divergence and possibly higher output power.
A suitable scheme for surface emission was proposed by Avetisyan and Kocharian [50] and experimentally demonstrated for fs-lasers by C. Weiss et al. [47]. An analytical expression for the expected THz frequency for a given poling period Λ and observation angle Θ has

already be given with Eqn. (5). From that equation it is obvious that a changed observation angle for a fixed poling period results in a changed THz frequency. This can be used to tune the THz radiation by changing the angle of observation. But note that this is very different compared to the method used for the frequency tuning in section 4.1.1. While for the approach in section 4.1.1 the crystal is rotated, for the method discussed in this section the angle of observation is changed. In the first case all participating waves propagate in forward direction (collinear setup) where as in the second case only the NIR wave propagates in forward direction while the THz wave is observed under an angle of Θ (non collinear setup).

Fig. 14 shows the calculated tuning curve for a poling period of $\Lambda = 127\mu m$. The angles $\Theta = 0$ and $\Theta = \pi$ correspond to THz radiation in the forward and backward direction, respectively. These observation directions have been discussed in detail in section 4.1. From Fig. 14 it is clear that for an angle of $\sim 63\,^{\circ}$ a singularity exists. This angle is the Cherenkov angle (see Eqn. (3)) discussed in section 3.2. For this angle not a single frequency but broadband radiation THz is emitted.

Similar to the generation of Cherenkov radiation the possible angle for the extraction of the THz radiation is limited, due to total internal reflection. The angles for which the generated THz radiation can leave the crystal (besides the forward and backward direction) are marked in Fig.14 by the grey box. Therefore we will focus the following discussion to this window.

For the experimental realization the sideways geometry scheme (using mirror set Ms, see Fig. 1) was used. The setup is very similar to the setup for the generation of Cherenkov radiation. Only the crystal was replaced and the focussing as well as the detection angle was adjusted for the detection of sideways radiation under the appropriate angle. For this experiment a 8 mm long crystal with a poling period of 127 μm was used. Fig. 15 (a) shows the experimentally obtained electric field of the generated pulse.

The Fourier transform results in the spectrum, which is shown in Fig. 15 (b). The spectrum is centered around 0.94 THz. This result differs from the theoretically expected value of 1.027 THz, which was obtained from Eqn. (5) for $\Theta = \frac{\pi}{2}$ and $\Lambda = 127\mu m$. But for an observation angle of 92.3° the expected center frequency matches the experimentally measured one. A variation of the observation angle of 2.3° is within the experimentally accuracy and explains the difference. In the right edge of the spectrum a dip caused by absorption of water vapor is obvious.

The measured relative bandwidth of the THz radiation is 10% (FWHM). This value is much larger than the theoretically expected value of 2%, which was calculated by Eqn.(7). The reason for this difference is the sensitivity of the THz frequency to changes in the observation angle and the sensitivity of the detector. This can clearly be seen from Fig. 14. Due to the finite detection angle $\Delta\Theta$ around the observation angle Θ_0 the THz radiation consists of various frequency components around the designed center frequency. An equation for the relative bandwidth can be obtained from Eqn. (5):

$$\frac{\Delta\nu}{\nu} = \frac{n_{THz}\sin\Theta_0}{|n_g - n_{THz}\cos\Theta_0|} \cdot \Delta\Theta. \tag{8}$$

This equation becomes zero for forward and backward radiation and infinite for the Cherenkov angle Θ_C, due to the $\sin\Theta_0$ and $\cos\Theta_0$ terms. In the surface emitting scheme the finite detection angle has to be considered. The parabolic mirrors used in the experimental setup have a typical collection angle of $\Delta\Theta = 15°$. With Eqn. (8) this results in an expected bandwidth of 11%, which is in good agreement with the measurement [47]. Therefore the bandwidth in the sideways emission scheme is mainly limited by the collection angle and can be adjusted suitable for a particular application. A reduction of the bandwidth in the surface emitting scheme can be obtained by using slits behind the ppLN.

5 Aperiodically poled lithium niobate (AppLN)

Up to now we discussed broadband THz radiation obtained by non phase matched DFG, Cherenkov type radiation and narrowband THz radiation obtained by quasi phase matched DFG in ppLN. Single cycle broadband as well as tunable narrowband THz radiation have attracted great interest for wide variety of applications. Beyond these possibilities the use of aperiodically poled crystals opens the opportunity to predefine the shape of the temporal or spectral envelope of the THz radiation or to tune the frequency of the THz radiation generated in sideways direction.

We will focus to the possibility to define the temporal or spectral shape of the THz radiation. A defined shape of the spectrum can be obtained by predefining a chirp of the fs-pulse and using a ppLN [48] or by using an unmodified fs-pulse together with an aperiodically poled LN (AppLN). For many applications a complex scheme to prechirp the fs-pulse according to the needs is not wise. But the use of aperiodically poled LN allows to use standard fs-pulses.

To understand the idea of using AppLN for this purpose, it is instructive to remember the way THz radiation is generated in ppLN. The electrical field in the time and frequency domain is determined by the superposition of the waves generated in the particular domains[46]. This can be clearly verified by Eqn. (33) obtained in part one. The generated spectrum is very sensitive to changes in the domain structure. Even small deviations from the predefined domain structure can be sensitively detected. Lee et al. [51] demonstrated this method. Due to this strong dependency a predefined domain structure can be used to define the THz spectrum. This was proposed

and experimentally demonstrated by Lee et al. [52,53]. A theoretical treatment has been published by Liu et al. [54]. But these discussions focus on the THz generation in AppLN in forward direction. This has the disadvantage that for the different frequency components as well as for the partial waves generated in different positions in the sample a significant varying absorption losses occur (see Fig. 9). Therefore only the remaining part of the radiation contributes to the interference.

The surface scheme which has already discussed for ppLN (see section 4.2) does not show this problem due to the short path length inside the medium. In addition AppLN may be of particular interest for easy frequency tuning in the surface emitting scheme. Therefore we will focus exemplary the discussion to this scheme.

While for bulk LN the length of the sample and for ppLN the length and the periodicity are adequate parameters to characterize the crystal for AppLN the particular aperiodic structure has to be considered. To allow a discussion we further focus exemplary to a special aperiodic structure. In Fig. 17 the photograph and the schematic of the selected AppLN is shown. The sample was poled with a poling period varying from 20 to 254 microns in steps of 13 microns. Each period is repeated 4 times.

The used experimental setup for the experiments was similar to the one used for common ppLN in the surface emitting scheme discussed in section 4.2. The upper graph of Fig. 18 (a) shows the experimentally obtained electric field of the generated pulse and the lower graph Fig. 18 (b) indicates the corresponding poling period. For every domain pair, one cycle in the electric field is generated. Four cycles in the electrical field corresponds to 4 domain pairs with the same period. As expected from the theoretical discussion[1] every single cycle of the electrical field can be predefined by the poling structure. But this means in accordance to Lee et al.[51–53] that the shape of the electrical field (eg. a linear or quadratically chirp) can be predefined, if the QPM structure of the AppLN is designed accordingly.

A further application of aperiodic structures may be the arrangement of various sets of different poling periods one after another to allow easy frequency tuning in the surface emitting scheme. While the forward scheme has to deal with strong absorption, the surface emitting scheme is limited by the focal length. Only in short range around the focal point emission in the sideways direction can be obtained (see section 4.2). By defining the position of the focal point of the fs radiation the contributing periods can be selected. This opens a way to overcome one of the remaining limitations of the surface emitting scheme discussed in section 4.2, which is the limit to one or two poling periods near the surface of the crystal. By arranging the various poling periods one after another and adjusting the position of the focus a similar tuning can be obtained in AppLN as in ppLN operated in forward direction.

5.1 Tilted periodically poled lithium niobate (TppLN)

THz beams generated in ppLN with standard collinear interaction schemes (see section 4) suffer an essentially reduced output efficiency due to the high absorption. The surface emitting scheme has been offered and demonstrated as an alternative (see section 4.2) to reduce the absorption losses. The main condition which has to be fulfilled was that the optical beam can be focused sharply enough so that the waist diameter is kept smaller than the expected wavelength of the THz radiation. Otherwise the phase shift between the THz rays generated at different points of the optical beam cross section along the observation direction may exceed 180°. In this case the different rays would interfere destructively in the detection point.

Because of the damage threshold this condition limited the permitted pump power. Correspondingly lower THz power could be achieved. In the case when longer (e.g. nanosecond) optical pulses should be used, the mentioned limitation could even make the utilization of the surface emitting scheme impossible. One has to note as well that since the smaller waists could be achieved only by sharper focusing, less number of domains could participate in the generation process, and a less monochromatic THz wave is detected (see section 4.2).

To eliminate the mentioned disadvantages a modified ppLN crystal for surface emitted THz wave generation was used. Mainly two poling structures have been discussed and demonstrated for this purpose. A sketch of the poling structure for both schemes is shown in Fig.19(a) and Fig.19(c). Beside a chessboard type poling structure a periodical domain structure oriented under an angle to the crystal edges so-called tilted-ppLN (TppLN) or slant-stripe-type has been discussed. Since both schemes are very similar in their impact on the THz generation we focus exemplary to the TppLN scheme. The main idea of the modification is the following: The input and output edges of the rectangular crystal are not cut parallel or perpendicular to the domains of the poled structure but under an angle α as depicted in Fig. 19(a). TppLN crystals has been successfully used for surface-emitted THz wave generation via difference-frequency mixing of optical waves in the nanosecond duration regime[55] and for the optical rectification of 100-fs pulses at 0.78 μm.

For the experimental demonstration the same setup is used as for the experiments with conventional ppLN in the surface emission scheme in section 4.2. Only the rectangular ppLN crystal has been substituted by a ppLN crystal with tilted periods. The angle α and poling period Λ (the double domain length) were determined from the quasi-phase-matching conditions in both x and y directions [1]:

$$\alpha = \arctan\left(\frac{n_{THz}}{n_g}\right) \tag{9}$$

$$\Lambda = \frac{c}{\nu} \cdot \frac{\sin\alpha}{n_g} \tag{10}$$

where ν is the desired frequency of the THz wave. A sketch of the definition of α and Λ is shown in Fig. 19 (b).
With $n_g = 2.3$ and $n_{THz} = 5.17$ for the generation of 1 THz Eqn. (9) and Eqn. (10) result in a poling period of $\Lambda = 56.2\mu$m and an angle of $\alpha = 24°$.
To get a THz-wave generation around 1 THz in the surface emitting geometry one needs a poling period of 130 μm in the standard orientation (regular ppLN) and a focusing of the pump beam down to a $10\mu m$ to $20\mu m$ waist size. A typical waveform of a THz-wave generated by such a regular ppLN is shown in Fig. 15 (a). A spherical lens (f=10 mm) was used to generate the shown wave-form around 1 THz. When the spherical lens is substituted by a cylindrical lens of also 10 mm focal length, a similar waveform is generated only when the curvature of the lens lay in the XY-plane. If, in contrary, the curvature was in the YZ-plane (the beam is not focused along y) then the measured THz radiation is too week and have a much lower frequency, corresponding to the backward generation as shown in Fig. 20(a) (see also Fig. 14).
After the regular ppLN was substituted by another one with tilted domains under an angle of $\alpha = 23°$ with a period of $\Lambda = 50\mu$m (close to the calculated values by Eqn. (9) and Eqn. (10)), a stronger emission and a higher frequency (around 1 THz) is generated (Fig. 20(b)). The parameters of the ppLN crystal are selected so, that along the y axis the THz rays generated from neighboring domains interfere constructively. Therefore the beam size along the y axis has not necessarily to be smaller than the generated wavelength. In that case, the phase difference between the rays generated from different parts of the beam cross section is quasi compensated by the periodical poled nonlinearity of the crystal in x direction, hence leading to those rays to interfere constructively at the detection point. The demonstrated possibility of using not very sharply focused pump beam with the tilted ppLN allows in addition for a bigger number of poling domains to be involved in THz generation process, resulting in a more monochromatic radiation. For demonstration a spherical lens with a focal length of 200 mm in combination with the same tilted ppLN sample was used. The focal spot size in that case would not be small enough to generate high frequency THz components in the regular ppLN sample and is demonstrated in Fig. 21 (a). In the case of tilted ppLN the same focusing geometry generates higher spectral components and stronger amplitude Fig. 21 (b).

6 Conclusion

In conclusion we have discussed theoretically and experimentally and compared various schemes to generate THz radiation in optical nonlinear crystals using fs-NIR-radiation. These schemes allow to produce broadband as well as narrowband but tunable THz radiation.
Following the outline of part one[1] we discussed the generation of THz radiation in bulk LN. While optical rectification is not efficient, due to the missing phase-matching, Cherenkov radiation is a suitable scheme to produce broadband radiation. The major task to obtain Cherenkov radiation efficiently is to extract the radiation from the crystal, because the Cherenkov angle is greater than the angle of internal total reflection. Two schemes (wedged crystals and silicon prims) to overcome this problem have been discussed and compared.
To obtain a reasonably amount of Cherenkov radiation it is necessary to sharply focus the NIR beam into the LN crystal, due to fullfill momentum conservation. For power scaling it is advantageous to use the tilted pulse front geometry to overcome the problem of optical damage of the crystal.
A very different and versatile approach to obtain phase matching is to use ppLN crystals. This scheme leads to narrowband but tunable radiation. Realizations in forward as well as in the surface/sideways emitting scheme and possibilities to tune the frequency of the THz radiation have been discussed. The surface emitting scheme has the benefit that the emitted radiation is generated close to the surface. Therefore only very low absorption losses occur. A promising solution to the necessary sharp focussing to obtain surface emitted radiation was the use of two dimensionally structured LN samples.
Aperiodically poled LN has been demonstrated to be a versatile possibility to design the electrical field as well as the frequency spectrum of the THz pulse.
Despite the discussion was focused on LN, these results can easily be applied to other nonlinear materials like GaAs, which has a strongly reduced absorption coefficient at THz frequencies.

Acknowledgments

The authors acknowledge Alexander Quosig for his help in preparation of samples for the experiments.

References

1. J. A. L'huillier, G. Torosyan, M. Theuer, Y. Avetisyan, and R. Beigang, to be published (2006).
2. K. Kawase, M. Sato, T. Taniuchi, and H. Ito, Appl. Phys. Lett. **68**, 2483 (1996).
3. A. Stepanov, J. Hebling, and J. Kuhl, Appl. Phys. B **81**, 23 (2005).
4. Y. Avetisyan, Y. Sasaki, and H. Ito, Appl. Phys. B **73**, 511 (2001).
5. J. Hebling, A. Stepanov, G. Almaasi, B. Bartal, and J. Kuhl, Appl. Phys. B **78**, 593 (2004).
6. M. Theuer, G. Torosyan, C. Rau, R. Beigang, K. Maki, C. Otani, and K. Kawase, Appl. Phys. Lett. **88**, 071122 (2006).

7. C. Weiss, G. Torosyan, J. Meyn, R. Wallenstein, R. Beigang, and Y. Avetisyan, Opt. Exp **8**, 497 (2001).
8. A. Stepanov, J. Kuhl, I. Kozma, E. Riedle, G. Almasi, and J. Hebling, Opt. Exp **13**, 5762 (2005).
9. P. Jepsen, C. Winnewisser, M. Schall, V. Schyja, S. Keiding, and H. Helm, Phys. Rev. E **53**, R3052 (1996).
10. A. Rice, Y. Jin, X. F. Ma, X. C. Zhang, D. Bliss, J. Larkin, and M. Alexander, Appl. Phys. Lett. **64**, 1324 (1994).
11. D. Zheng, L. A. Gordon, Y. S. Wu, R. S. Feigelson, M. M. Fejer, R. L. Byer, and K. L. Vodopyanov, Opt. Lett. **23**, 1010 (1998).
12. W. Shi, Y. Ding, N. Fernelius, and K. Vodopyanov, Opt. Lett. **27**, 1454 (2002).
13. W. Shi and Y. Ding, Appl. Phys. Lett. **84**, 1635 (2004).
14. W. Shi, Y. J. Ding, and P. G. Schunemann, Opt. Commun. **233**, 183 (2004).
15. K. Kawase, M. Mizuno, S. Sohma, H. Takahashi, T. Taniuchi, Y. Urata, S. Wada, H. Tashiro, and H. Ito, Opt. Lett. **24**, 1065 (1999).
16. K. Kawase, T. Hatanaka, H. Takahashi, K. Nakamura, T. Taniuchi, and H. Ito, Opt. Lett. **25**, 1714 (2000).
17. A. Nahata, D. H. Auston, C. J. Wu, and J. T. Yardley, Appl. Phys. Lett. **67**, 1358 (1995).
18. A. Sinyukov, M. Leahy, L. Hayden, M. Haller, J. Luo, A. Jen, and L. Dalton, Appl. Phys. Lett. **85**, 5827 (2004).
19. D. A. Roberts, IEEE. J. Quantum. Electron. **28**, 2057 (1992).
20. A. Harada and Y. Nihei, Appl. Phys. Lett. **69**, 2629 (1996).
21. L. E. Myers, R. C. Eckardt, M. M. Fejer, and R. L. Byer, Opt. Lett. **21**, 591 (1996).
22. G. D. Miller, *Periodically poled lithium niobate: Modelling, fabrication, and nonlinear-optical performance*, PhD thesis, Stanford University, 1998.
23. M. Yamada, N. Nada, M. Saitoh, and K. Watanabe, Appl. Phys. Lett. **62**, 435 (1993).
24. L. Palfalvi, J. Hebling, J. Kuhl, A. Peter, and K. Polgar, J. Appl. Phys. **97**, 123505 (2005).
25. M. Schall, H. Helm, and S. Keiding, Int. J. Infrared Millimeter Waves **20**, 595 (1999).
26. D. A. Bosomword, Appl. Phys. Lett. **9**, 330 (1966).
27. H. J. Bakker, S. Hunsche, and H. Kurz, Phys. Rev. B **50**, 914 (1994).
28. J. ichi Shikata, M. Sato, T. Taniuchi, H. Ito, and K. Kawase, Opt. Lett. **24**, 202 (1999).
29. M. Bass, P. A. Franken, J. F. Ward, and G. Weinreich, Phys. Rev. Lett. **9**, 446 (1962).
30. A. Nahata, A. S. Weling, and T. F. Heinz, Appl. Phys. Lett. **69**, 2321 (1996).
31. L. Xu, X. C. Zhang, and D. H. Auston, Appl. Phys. Lett. **61**, 1784 (1992).
32. T. J. Carrig, G. Rodriguez, T. S. Clement, A. J. Taylor, and K. R. Stewart, Appl. Phys. Lett. **66**, 121 (1995).
33. G. A. Askaryan, Sov. Phys. JETP **15**, 943 (1962).
34. D. H. Auston, K. P. Cheung, J. A. Valdmanis, and D. A. Kleinman, Phys. Rev. Lett. **53**, 1555 (1984).
35. D. A. Bagdasaryan, A. H. Makaryan, and P. Pogosyan, JETP. Lett **37**, 594 (1983).
36. B. B. Hu, X. C. Zhang, and D. H. Auston, Appl. Phys. Lett. **56**, 506 (1990).
37. K. Kawase, M. Sato, K. Nakamura, T. Taniuchi, and H. Ito, Appl. Phys. Lett. **71**, 753 (1997).
38. D. Grischkowsky, S. Keiding, M. van Exter, and C. Fattinger, J. Opt. Soc. Am. B **7**, 2006 (1990).
39. G. D. Boyd and D. A. Kleinmann, J. Appl. Phys. **39**, 3597 (1968).
40. M. M. Fejer, G. A. Magel, D. H. Jundt, and R. L. Byer, IEEE. J. Quantum. Electron. **28**, 2631 (1992).
41. J. Meyn, M. Klein, D. Woll, R. Wallenstein, and D. Rytz, Opt. Lett. **24**, 1154 (1999).
42. R. Huber, A. Brodschelm, F. Tauser, and A. Leitenstorfer, Appl. Phys. Lett. **76**, 3191 (2000).
43. J. Hebling, G. Almasi, I. Kozma, and J. Kuhl, Opt. Exp **10**, 1161 (2002).
44. Y. Lee, T. Meade, M. DeCamp, T. Norris, and A. Galvanauskas, Appl. Phys. Lett. **77**, 1244 (2000).
45. Y. Lee, T. Meade, V. Perlin, H. Winful, T. Norris, and A. Galvanauskas, Appl. Phys. Lett. **76**, 2505 (2000).
46. Y. Lee, T. Meade, T. Norris, and A. Galvanauskas, Appl. Phys. Lett. **78**, 3583 (2001).
47. C. Weiss, G. Torosyan, Y. Avetisyan, and R. Beigang, Opt. Lett. **26**, 563 (2001).
48. J. Ahn, A. Efimov, R. Averitt, and A. Taylor, Opt. Exp **11**, 2486 (2003).
49. U. Strossner, J. Meyn, R. Wallenstein, P. Urenski, A. Arie, G. Rosenman, J. Mlynek, S. Schiller, and A. Peters, J. Opt. Soc. Am. B **19**, 1419 (2002).
50. Y. H. Avetisyan and K. N. Kocharian, A new method of terahertz difference frequency generation using periodically poled waveguide, in *CLEO 1999 Technical Digest*, pp. 380–381, 1999.
51. Y. S. Lee, T. Meade, M. L. Naudeau, T. B. Norris, and A. Galvanauskas, Appl. Phys. Lett. **77**, 2488 (2000).
52. Y. Lee and T. Norris, J. Opt. Soc. Am. B **19**, 2791 (2002).
53. Y. Lee, N. Amer, and W. Hurlbut, Appl. Phys. Lett. **82**, 170 (2003).
54. X. Liu, J. Wu, W. Duan, and B. Gu, J. Appl. Phys. **97**, 114108 (2005).
55. Y. Sasaki, Y. Avetisyan, K. Kawase, and H. Ito, Appl. Phys. Lett. **81**, 3323 (2002).

Figures

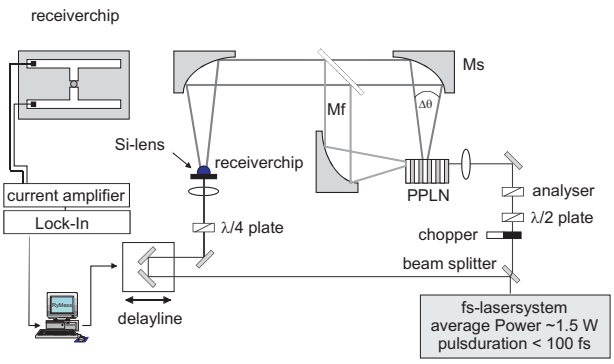

Fig. 1 Experimental setup for the generation and detection of THz radiation. With this setup the radiation in forward direction as well as the radiation in sideways direction (surface emission or Cherenkov like radiation) can be investigated.

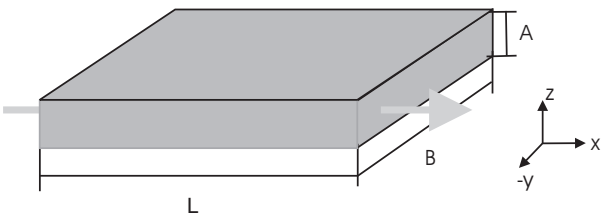

Fig. 2 Scheme of the sample and coordinate system used for the THz generation in bulk LN

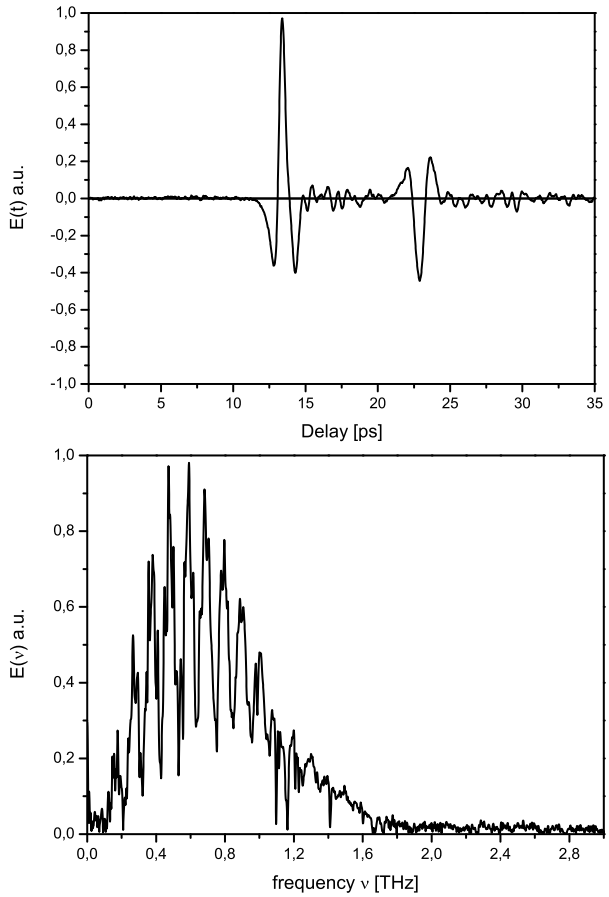

Fig. 3 Optical rectification (non phasematched DFG): (a) electrical field and (b) frequency spectrum

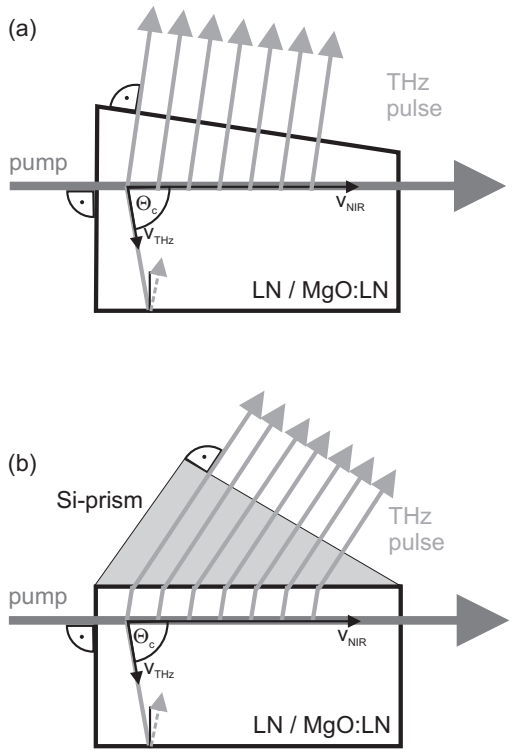

Fig. 4 Schematically diagram of the crystal shape for the extraction of Cherenkov type THz radiation: a) Crystal with a wedged surface b) Crystal with a silicon prism

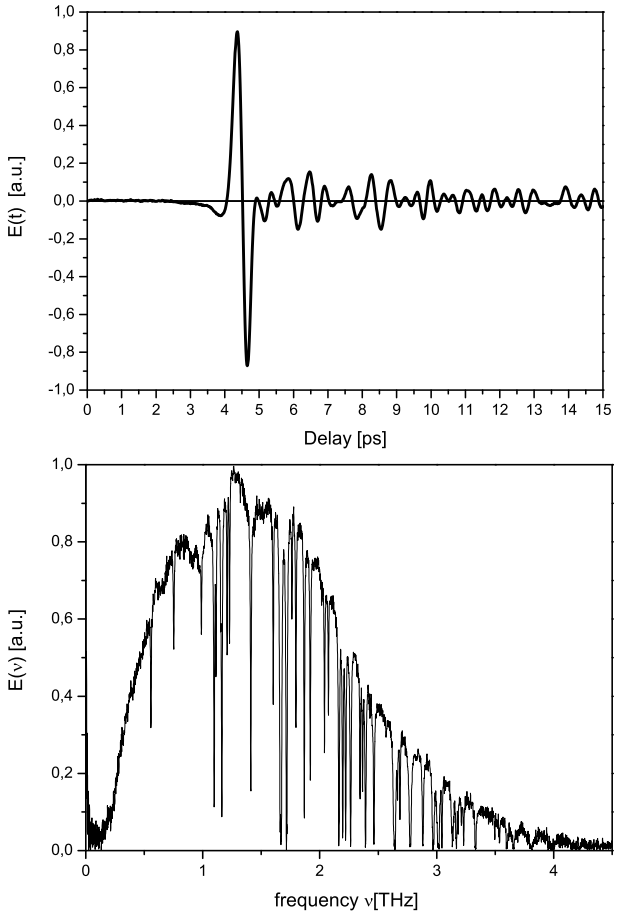

Fig. 5 Cherenkov radiation (a) Single-cycle electrical field (b) frequency spectrum for a wedged LN sample

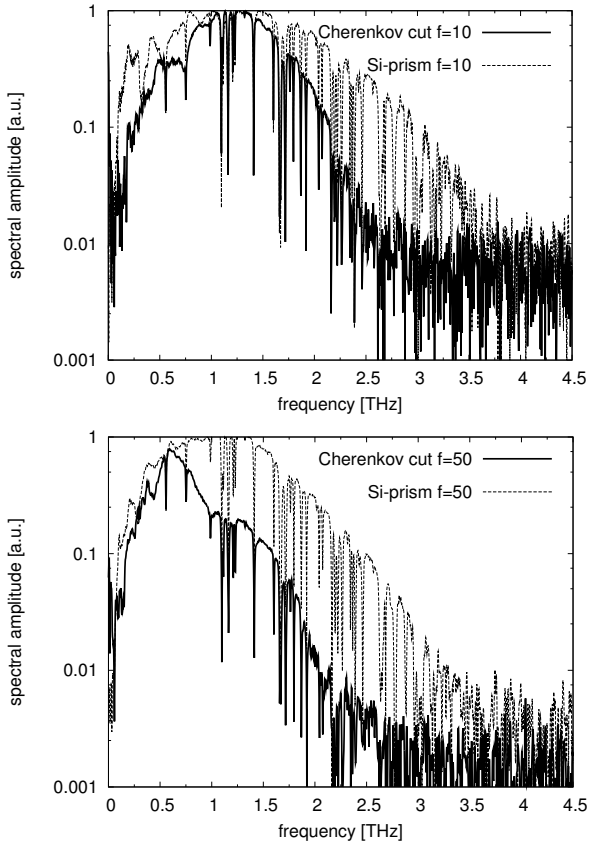

Fig. 6 Measured Cherenkov type THz spectra for wedged MgO:LN(solid line) and a Si-prism output coupling (dotted line) for different focal length (a) f=10mm (b) f=50 mm

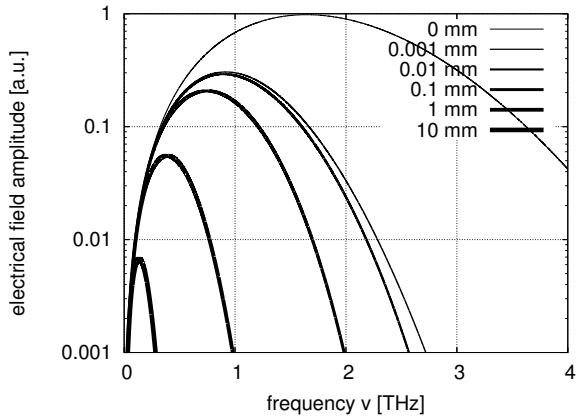

Fig. 7 Calculated spectra for different path length inside LN, a pulse duration of $\tau = 100$ fs, a beam waist of $\omega_0 = 30$ μm and the absorption coefficient obtained by M. Schall et al.[25]

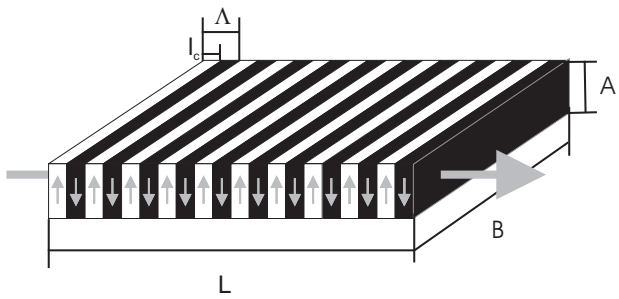

Fig. 8 Scheme of the samples typically used for the THz generation in periodically poled LN (ppLN)

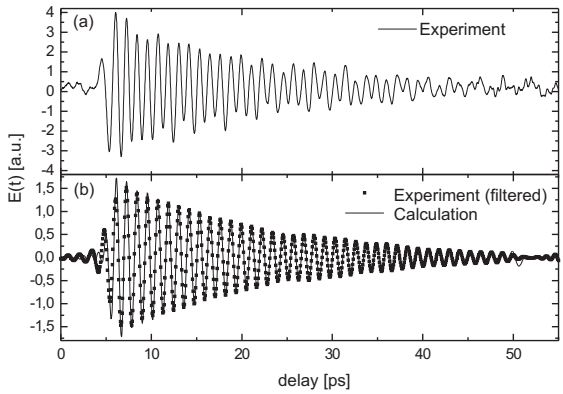

Fig. 9 (a) Experimentally and (b) theoretically obtained electrical field of the THz radiation generated in forward direction in a ppLN with a poling period of $120\mu m$.

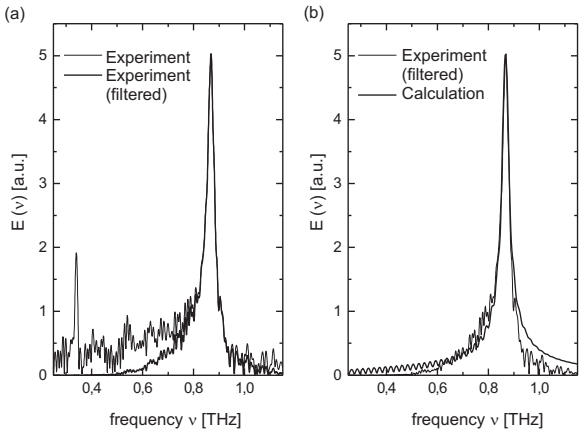

Fig. 10 (a) Experimentally and (b) theoretically obtained spectra of the THz radiation generated in forward direction in a ppLN with a poling period of $120\mu m$.

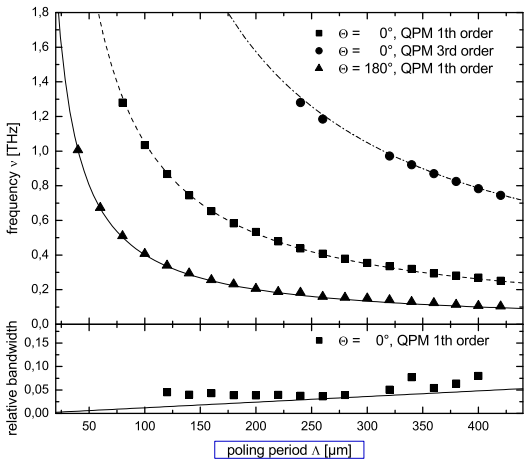

Fig. 11 Experimentally obtained (a) THz frequencies and (b) bandwidth depending on the poling period for emission in forward direction ($\Theta = 0°$) and backward direction ($\Theta = 180°$).

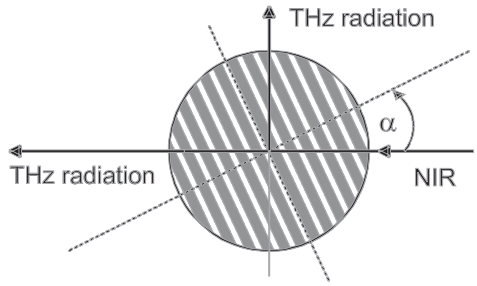

Fig. 12 Schematic diagram of the circular ppLN crystal used for continuous frequency tuning

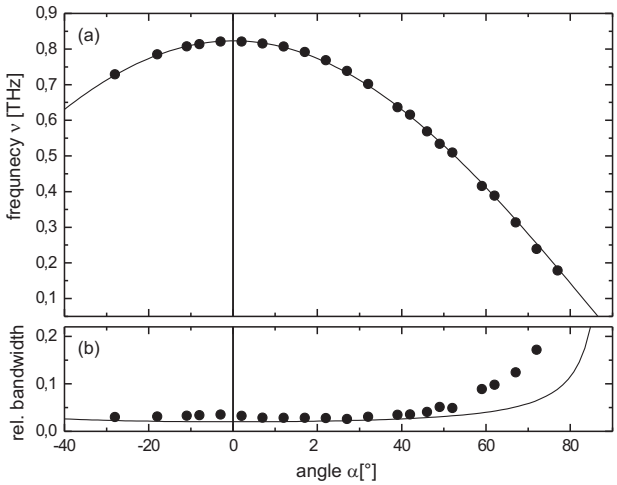

Fig. 13 (a) THz frequency observed in forward direction as a function of the angle between the direction of propagation and the poling structure. The solid line represents the theoretically obtained tuning characteristic. (b) relative bandwidth for different propagation angles. The solid line represents the calculated relative bandwidth, assuming a rectangular waveform.

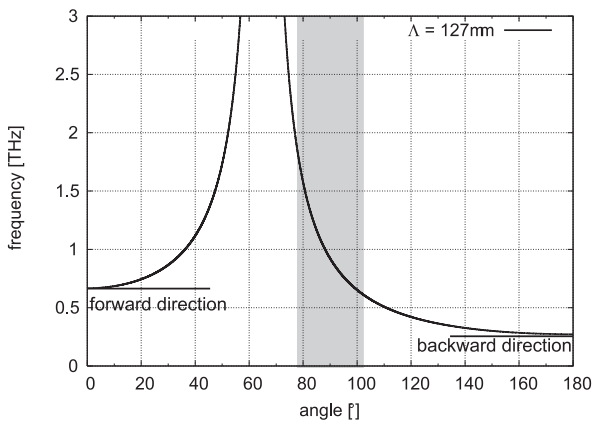

Fig. 14 Dependency of the difference frequency ν on the angle between the propagation direction of the NIR and THz beam.

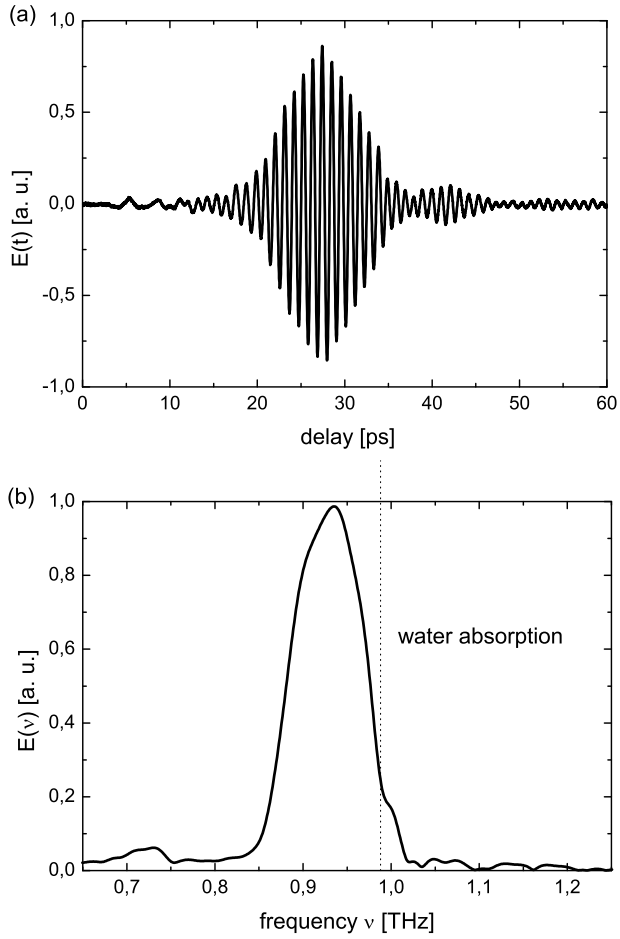

Fig. 15 Experimentally obtained electrical field (a) and frequency spectrum (b) of the THz radiation generated in surface emission geometry in a ppLN with a poling period of $127\mu m$.

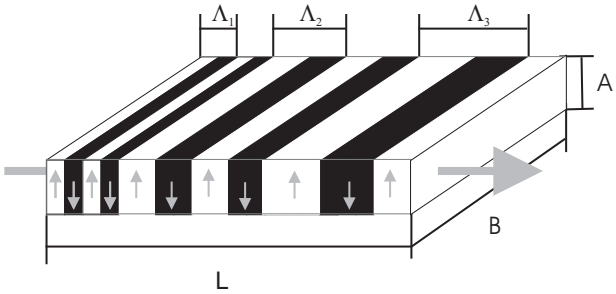

Fig. 16 Exemplary poling structure for the THz generation in aperiodically poled LN (AppLN)

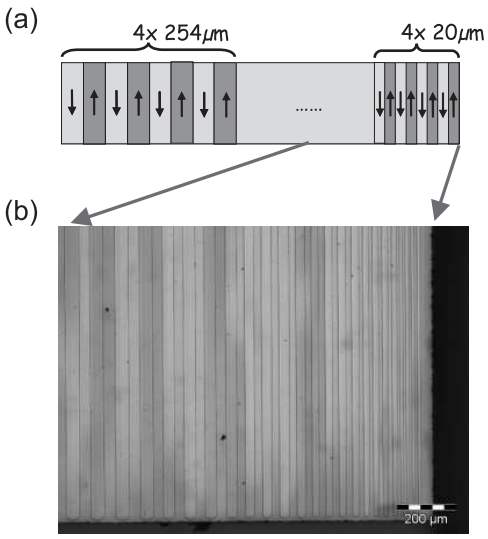

Fig. 17 Schematic (a) and photograph (b) of an AppLN for the THz generation in surface emission geometry.

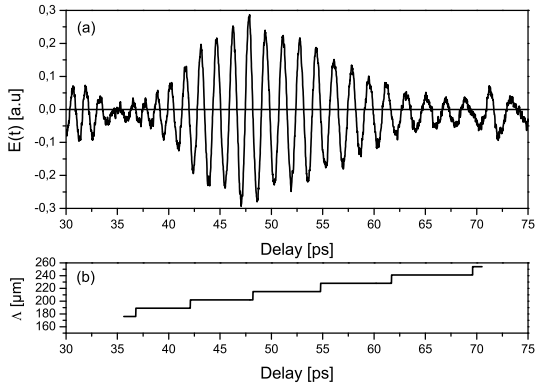

Fig. 18 Experimentally obtained a) electrical field amplitude for an AppLN and b) designed poling period for the AppLN.

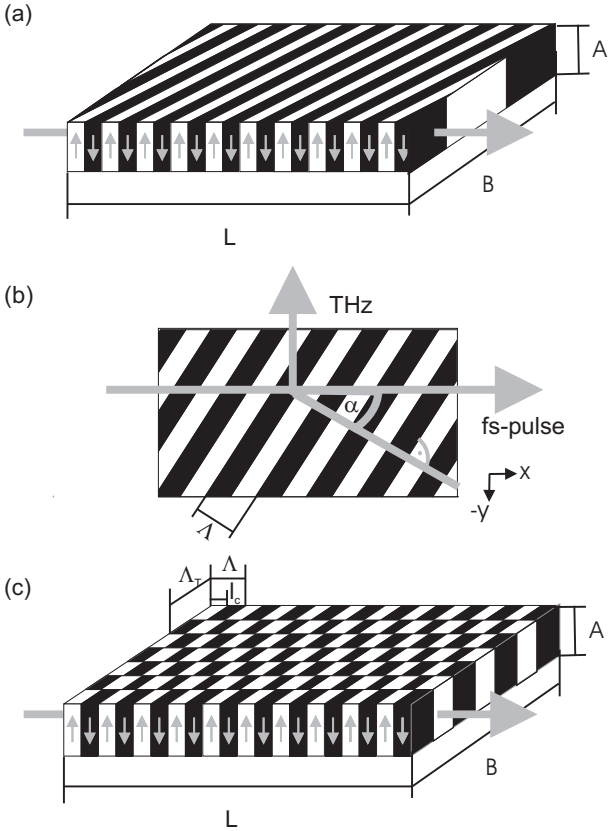

Fig. 19 The two typically used poling structures to enhance the THz radiation output in the surface emission scheme: (a)/(b) slant stripe type (c) chessboard type. In (b) a sketch of the slant stripe type with the definition of the angle α and the poling period Λ is shown

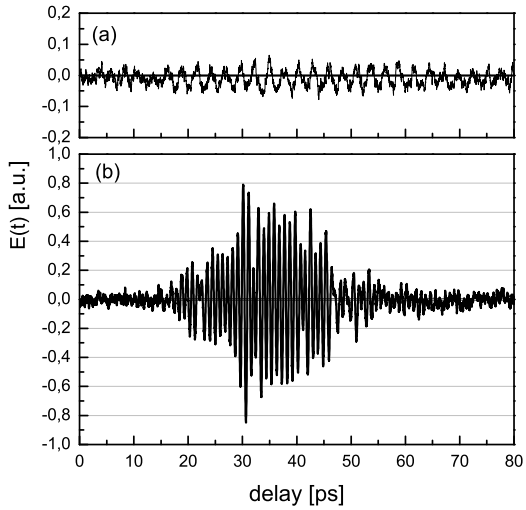

Fig. 20 Experimentally obtained electrical field for a focussing of the fs-pulse in the XZ-plane with a cylindrical lens (f=10mm) in (a) regular ppLN and (b) TppLN.

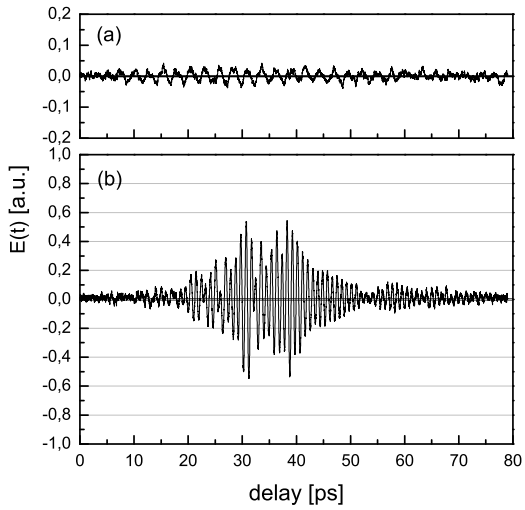

Fig. 21 Experimentally obtained electrical field for a focussing of the fs-pulse with a spherical lens (f=200mm) in (a) regular ppLN and (b) TppLN.